A Low-Profile Energy Selective Surface With Ultra-Wide Absorption Band

Wenjian Gong, Wenmei Zhang, *Senior Member, IEEE*, Xinwei Chen, Guorui Han, Liping Han, Jinrong Su, and Rongcao Yang

***Abstract*— A low-profile energy selective surface (ESS) with an ultra-wide absorption band is proposed in this article. It consists of a switchable layer and an absorptive layer. The switchable layer uses p-i-n diodes to adaptively adjust the operating mode. When the incident wave power is low, the ESS operates in transmission mode. It behaves as a bandpass frequency selective surface (FSS) having an ultra-wideband (UWB) absorption out of the passband. As high-power microwaves (HPMs) are incident, the ESS changes to shield mode. The HPM in the passband are reflected, while those out of band are absorbed. As a result, stealth and shielding are realized at the same time. By loading metal patches on both sides of the dielectric substrate, the number of transmission zero out of the passband is increased. As a result, the shielding and absorption bandwidth (AB) are widened. The wide absorption band can absorb detection signals before the diodes are triggered and provide a shield in advance. The experimental results show that the ESS has an insertion loss (IL) of 0.6 dB at 3.8 GHz and an absorption band range of 5.97–13.97 GHz in transmission mode. While in shield mode, a shielding effectiveness (SE) of 13 dB and an absorption band range of 5.74–12.82 GHz are obtained. This novel ESS simultaneously achieving high-power electromagnetic (EM) protection and stealth in a wide band has various prospects of applications in EM protection, EM compatibility, and EM interference along with stealth technology.**

***Index Terms*— Energy selective surface (ESS), high-power microwaves (HPMs), p-i-n diode, ultra-wideband (UWB) absorption.**

I. Introduction

In COMMUNICATION systems, the high-power microwave (HPM) is a great threat to electronic equipment. It can not only interfere with the working of electronic devices, but also bring down the entire communication equipment. Therefore, it is crucial to protect electronic devices from HPM. Traditional shielding methods have evolved from electromagnetic (EM) compatibility technologies, which mainly used metal plates to isolate HPM. However, normal communication signals were also blocked. With the development of EM shielding, many new technologies, such as the frequency selective surface (FSS) and energy selective surface (ESS) have emerged.

Manuscript received 28 May 2022; revised 10 August 2022; accepted 9 October 2022. Date of publication 29 November 2022; date of current version 6 March 2023. This work was supported in part by the National Science Foundation of China under Grant 62071282, in part by the Excellent Achievement Cultivation Project for Universities in Shanxi Province under Grant 2019KJ001, and in part by the Shanxi "1331 Project" Key Subjects Construction under Grant 1331KSC. *(Corresponding author: Wenmei Zhang.)*

The authors are with the School of Physics and Electronic Engineering, Shanxi University, Taiyuan, Shanxi 030006, China (e-mail: zhangwm@sxu.edu.cn).

Color versions of one or more figures in this article are available at https://doi.org/10.1109/TMTT.2022.3222385.

Digital Object Identifier 10.1109/TMTT.2022.3222385

FSS, as a spatial filter with good frequency selection characteristics, has been widely used in communication systems [1]. It can be made to achieve band-stop [2] or bandpass [3], [4] characteristics. In recent years, FSS has gradually evolved into the active FSS (AFSS) loaded with adjustable device, such as varactor diodes [5], [6], [7], [8], cantilever beam switches [9], and optically controlled silicon switches [10]. By adjusting the bias voltage and current of active devices, the EM characteristics of AFSS can be changed. The realized AFSSs have been utilized for oscillators, amplifiers, switches, phase shifters, mixers, frequency multipliers, and terahertz modulators [11], [12]. It should be mentioned that the AFSSs controlled by the bias circuit cannot reject HPM in the passband autonomously.

ESS, with the energy selection property in the passband, has been widely studied. Yang et al. [13], [14] proposed an ESS, which can be adaptively activated according to the electric field intensity of incident wave. It consisted of a dense array of p-i-n diodes and metal patches. In the range of 0.5–1.5 GHz, the low power signals can be transmitted. However, when the field intensity of incident wave reached 1300 V/m, the insertion loss (IL) of ESS increased rapidly. Zhou et al. [15] designed an ESS with hexagonal spiral patches, which achieved dual-band energy selection characteristics. Besides, it took triangle arrangement mode to restrain the grating lobe. In addition, the multi-layer structure has been implemented to increase the resonance points and obtain broadband shielding [16], [17].

The above-mentioned ESSs had a high reflection coefficient for the signal out of the passband. They were more likely to be detected and attacked. Therefore, it is crucial to study EM stealth for ESS. In order to obtain the broadband absorption out of the passband, Yuan et al. [18] introduced a lossy layer into the conventional ESS and realized the EM stealth. And Zhou and Shen [19] designed an absorptive ESS by loading rectangular absorbing materials inside the 3-D structure. However, their narrow absorption bands were insufficient to avoid ultra-wideband (UWB) detection and their profiles were also becoming higher.

In this article, a low-profile ESS with an ultra-wide absorption band is proposed. It enables to adaptively switch the

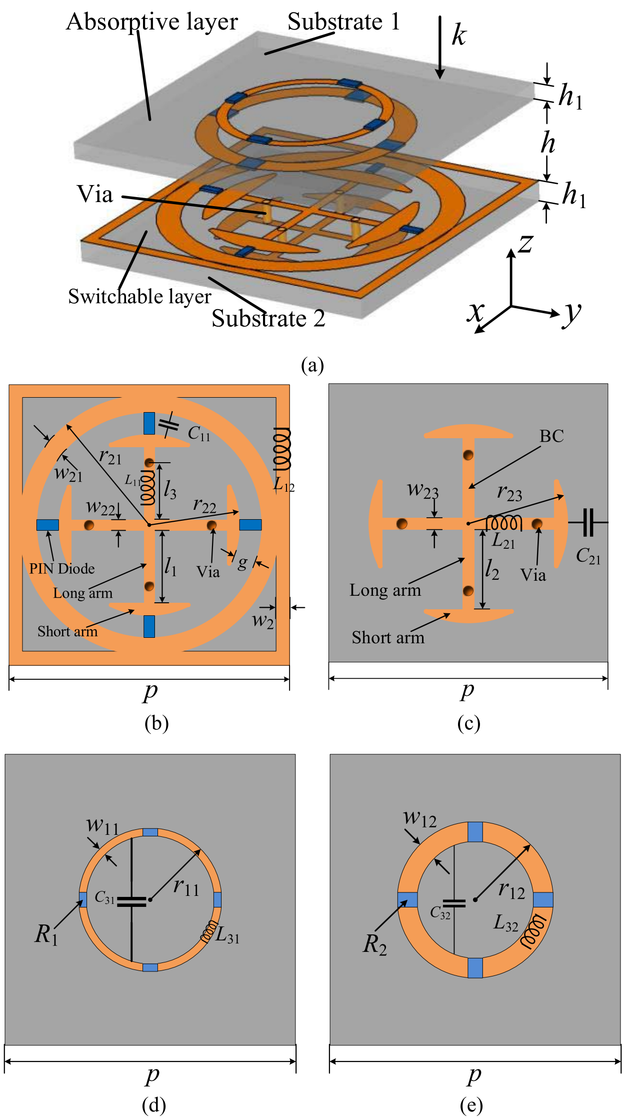

Fig. 1. Unit of proposed ESS. (a) 3-D view. (b) Front view of switchable layer. (c) Back view of switchable layer. (d) Front view of absorptive layer. (e) Back view of absorptive layer.

transmission/shield mode according to the incident power level in operating band. Besides, the ESS adopts a double-layer structure, so that a low profile of $0.08\lambda_0$ (λ_0 is the free-space wavelength at the operating frequency) is obtained. At last, a prototype of the ESS is fabricated, and the measured result shows that the signal can be transmitted in the range of 3.61–4.24 GHz at transmission mode, and be rejected in the range of 0–12.82 GHz at shield mode. Also, the relative bandwidths of the absorption bands in transmission/shield mode are 80% (5.97–13.97 GHz) and 76% (5.74–12.82 GHz), respectively. Comparing to the reported ESS [16], [18], [19], our ESS having wider ultra-wide absorption and protection band can block the high-intensity radiation field and EM pulse. Also, it possesses stealth function against the UWB EM wave.

II. Structure Design and Analysis

The unit of the proposed ESS is illustrated in Fig. 1(a). It consists of an absorptive layer and a switchable layer and

TABLE I

Optimized Dimensions of the ESS (unit: mm)

Symbol	Value	Symbol	Value
w_{11}	0.5	r_{11}	4.0
w_{12}	1.0	r_{12}	5.0
w_{21}	1.1	r_{21}	7.0
w_{22}	0.5	r_{22}	4.9
w_{23}	0.5	r_{23}	4.4
w_2	0.6	l_1	3.45
h	4.0	l_2	3.0
h_1	0.8	l_3	2.4
p	15.0	g	1.0

they are printed on a substrate 1 and 2 (flame retardant 4 (FR-4) dielectric substrate, $\varepsilon_r = 4.3$, $\tan\delta = 0.025$) with a thickness of h_1. Two layers are separated by an air layer with a thickness of h.

The switchable layer is formed by two layers of patches printed on both sides of substrate 2. On the front side, the nested square-ring, circle-ring, and deformed Jerusalem-cross patch as shown in Fig. 1(b) are printed and four p-i-n diodes (SMP1345-079LF) are arranged. In the back side, another cross patch [shown in Fig. 1(c)] is etched and it is connected to the patch in the front side through four vias. P-i-n diodes are controlled by the average power of the incident wave and no biasing circuits are required (operating principle of the p-i-n diode under microwave signal is shown in Appendix A). Under the normal low power signal, every diode is OFF and can be equivalent to a small capacitor ($C_{\mathrm{off}} = 0.15$ pF). The switchable layer can be equated to a bandpass FSS. The signals in the passband are transmitted with low loss, while those out of the passband are reflected. When illuminated by HPM with the average power exceeding the threshold, the p-i-n diode will be turned on and behaves as a small resistor ($R_{\mathrm{on}} = 1.5\ \Omega$) and inductor ($L_{\mathrm{on}} = 0.7$ nH) in series. All the HPM in operating band is rejected.

The unit of the absorptive layer is presented in Fig. 1(d) and (e). It is designed according to the Salisbury screen approach [20] and is formed by two circle-ring patches printed on the both sides of substrate 1. In order to absorb the energy of the EM wave, R_1 (400 Ω) and R_2 (50 Ω) are introduced at the gaps of the rings. Here, it is noted when the HPM is incident, a large amount of heat will be generated by resistors and metallic patches. Separately arranging two metal patterns on the upper and lower layers of the substrate is helpful to dissipate heat.

Finally, the ESS integrated absorptive and switchable layer are optimized using CST. The dimensions are shown in Table I. The optimization routine and technical details are indicated in Appendix B to avoid breaking the flow of the text. In Sections II-A and II-B, we will give the equivalent circuit modes of each part of ESS and analyze its performance. It should be stated that the designed ESS operates in several gigahertz (GHz) frequency band. Therefore, circuit modes can be phenomenological and assumed low frequency approximation. Also, the

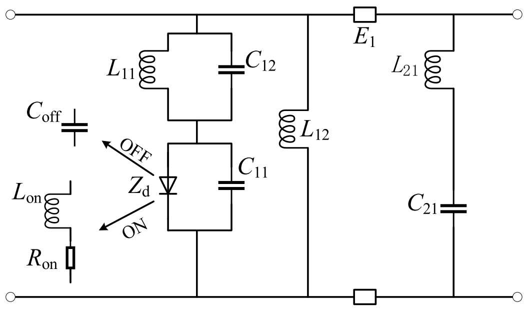

Fig. 2. Equivalent circuit model of switchable layer.

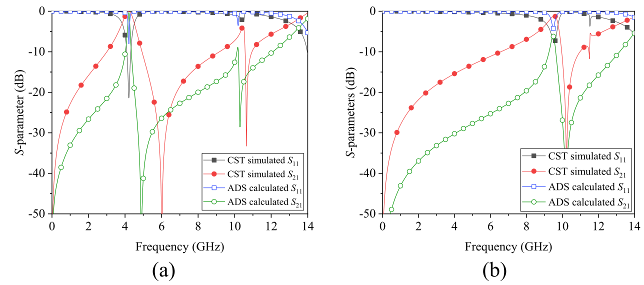

Fig. 3. Comparison of S-parameters from ADS and CST. (a) Diodes OFF. (b) Diodes ON.

full electrodynamic equivalent circuit [21] is beyond the scope of this article.

A. Design of Switchable Layer

Fig. 2 describes the equivalent circuit model of the switchable layer. On the front side, the long arm of the cross and the vias (take the capacitance formed by the patches connected to it into account) can be equivalent to L_{11} and C_{12}, respectively, while the short arm and inserted p-i-n diodes can be regarded as the paralleled C_{11} and Z_d. Further, the value of C_{11} and L_{11} can be approximated by r_{22}, g, l_1, and w_{22} as [22], [23]

$$C_{11} = \varepsilon_0 \varepsilon_{\text{eff}} \frac{2r_{22}}{\pi} \ln\left(\frac{1}{\sin \frac{\pi g}{2r_{22}}}\right) \tag{1}$$

$$L_{11} = \mu_0 \frac{4l_1}{\pi} \ln\left(\frac{1}{\sin \frac{\pi w_{22}}{4l_1}}\right) \tag{2}$$

where ε_0 and ε_{eff} are the dielectric constant in free space and the effective dielectric constant of substrate 2, respectively, μ_0 is the permeability in free space. In addition, the square-ring patch can be considered as a parallel L_{12}. On the back side, the long arm of the cross patch can be taken as L_{21}, while the gap between the adjacent units is equivalent to C_{21}. In addition, the substrate 2 can be considered as a transmission line with an electrical length of E_1.

Then, the values of each parameter calculated in advanced design system (ADS) are as follows: $L_{11} = 0.3$ nH, $C_{11} = 0.72$ pF, $L_{12} = 0.26$ nH, $C_{12} = 0.44$ pF, $L_{21} = 0.22$ nH, $C_{21} = 0.13$ pF, and $E_1 = 0.018$ (at 4.2 GHz). S-parameters calculated in ADS and simulated from CST are illustrated in Fig. 3. It can be seen from Fig. 3(a) that when diodes are cut off, the switchable layer resonates at 4.2 GHz and the signal in the passband can be transmitted. While the diodes are turned on, as shown in Fig. 3(b), S_{21} in the operating band are less than -10 dB. Further, the $L_{21}C_{21}$ connected in series resonates at about 10 GHz to form a transmission zero, thus widening the reflection bandwidth. The calculated result is in reasonable agreement with the simulated one, which proves the validity of the equivalent circuit model.

B. Design of Absorptive Layer

In order to study the absorption performance of the absorptive layer, we placed a metal plate $h = 4$ mm away from it and formed an absorber. The equivalent circuit model of the absorber is depicted in Fig. 4. The front and back circle-ring

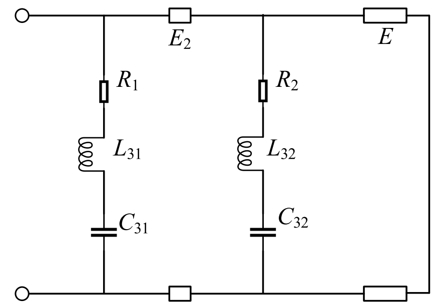

Fig. 4. Equivalent circuit model of the absorber.

patches are equivalent to two *RLC* series circuits. The values of L_{31}, L_{32}, C_{31}, and C_{32} can be approximated by the radius and width of the rings as [22], [23]

$$L_{3i} = \mu_0 \frac{2r_{1i}}{\pi} \ln\left(\frac{1}{\sin \frac{\pi w_{1i}}{2r_{1i}}}\right)\bigg|_{i=1,2} \tag{3}$$

$$C_{3i} = \varepsilon_0 \varepsilon_{\text{eff}} \frac{2(r_{1i} - w_{1i})}{\pi} \ln\left(\frac{1}{\sin \frac{\pi r_{1i}}{(r_{1i} - w_{1i})}}\right)\bigg|_{i=1,2} \tag{4}$$

where ε_0 and ε_{eff} are the dielectric constant in free space and the effective dielectric constant of substrate 1, respectively, μ_0 is the permeability in free space. The substrate 1 and the air layer can be regard as transmission lines with electrical lengths of E_2 and E, respectively.

Finally, the values of each parameter calculated in ADS are as follows: $L_{31} = 9.1$ nH, $C_{31} = 0.055$ pF, $L_{32} = 4.9$ nH, $C_{32} = 0.032$ pF, and $E = 0.056$, $E_2 = 0.018$ (at 4.2 GHz). The reflection coefficients calculated in ADS and simulated from CST are indicated in Fig. 5. The two series circuits resonate at 6.5 and 12 GHz and form two absorption peaks that the absorption bandwidth (AB) is widened. The reflection coefficient calculated in ADS is reasonable consistent with that simulated in CST.

C. ESS Performance

Replace the metal plate in the above absorbers with the switchable layer, and the ESS with an ultra-wide absorption band is accomplished. In order to obtain better shielding and absorption effect, the back-side cross (BC) patch is arranged and connected with the patch on the front side through vias. And the S-parameters of the ESS with/without BC and vias are shown in Fig. 6. When the low-power signal is incident, it can

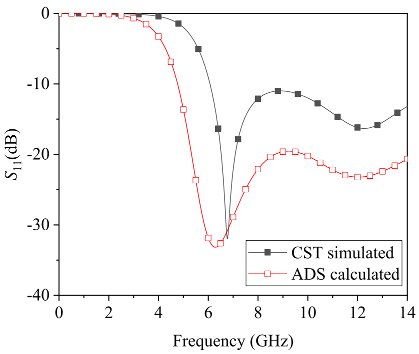

Fig. 5. Comparison of reflection coefficient from ADS and CST.

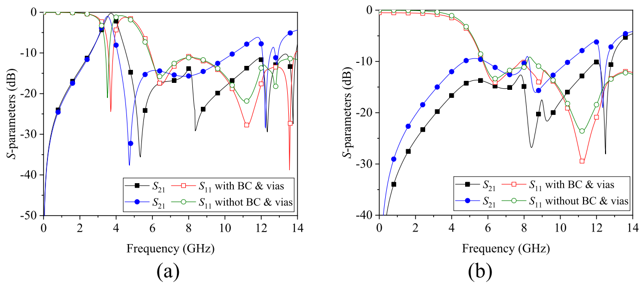

Fig. 6. S-parameters of ESS with and without BC and vias. (a) Low power signal incidence. (b) HPM incidence.

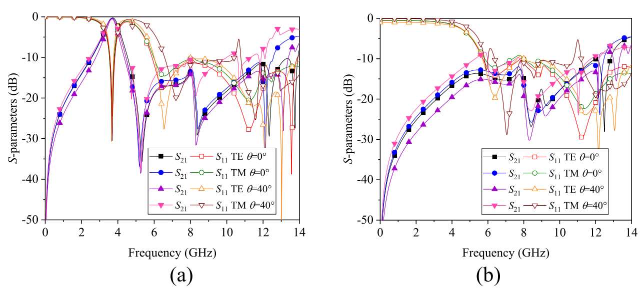

Fig. 7. S-parameters of ESS for different θ. (a) Low power signal incidence. (b) HPM incidence.

be observed from Fig. 6(a) that with loading BC and vias, a transmission zero at 8.2 GHz appears because every branch of the cross patch has a length of approximately 1/4λ_g (where λ_g is the wavelength of the guided wave at 8.2 GHz) and the resonance occurs at this frequency. So, transmission coefficient around it decreases significantly. Besides, S_{21} near 11.7 GHz is successfully suppressed below -10 dB, and the AB is expanded significantly. Conversely, when HPM is incident, as shown in Fig. 6(b), the transmission coefficient in the whole band is decreased due to the incorporation of BC and vias. Especially, S_{21} around 11.8 GHz is reduced to -11 dB. As a result, S_{21} is less than 10 dB from 0 to 12.8 GHz. According to the shielding effectiveness (SE) = ABS (S_{21}), it can be concluded that the corresponding relative bandwidth for SE $<$ 10 dB is 200%.

In practice, EM waves are mostly obliquely incident. Therefore, the S-parameters of ESS for different incidence angles θ (polarization angles $\varphi = 0°$) are explored and the results are given in Fig. 7. In Fig. 7(a), for TE polarized wave,

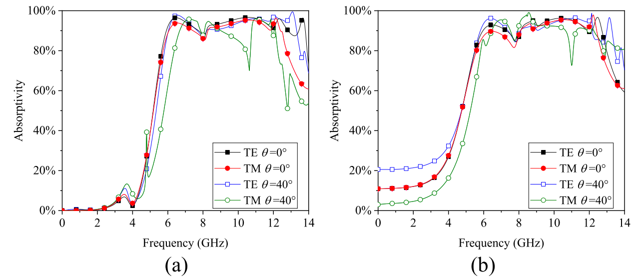

Fig. 8. Absorptivity of ESS for different θ. (a) Low power signal incidence. (b) HPM incidence.

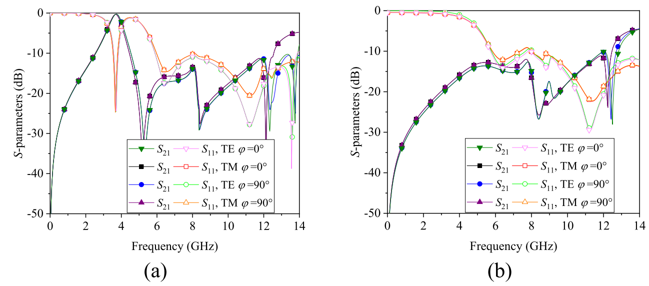

Fig. 9. S-parameters of ESS for different φ. (a) Low power signal incidence. (b) HPM incidence.

when the ESS is in transmission mode and $\theta = 0°$, the bandwidth for $S_{21} > -3$ dB is 680 MHz (3.39–4.07 GHz), in which the maximum IL is 0.2 dB at 3.72 GHz. Moreover, the AB (S_{21}, $S_{11} > -10$ dB) is 8 GHz (5.9–13.9 GHz). As θ increases from 0° to 40°, S_{21} and S_{11} basically unchanged. When HPM is incident, the diodes are triggered and the ESS turns to shield mode. As can be seen from Fig. 7(b), when $\theta = 0°$, the ESS can shield the signal ($S_{21} > -10$ dB) in the range of 0–12.82 GHz. The AB decreases to 7.08 GHz (5.74–12.82 GHz). With θ increases to 40°, the SE gradually increases, while the bandwidth of the absorption band decreases to 6.48 GHz (5.7–12.18 GHz). For TM polarized wave, the results are basically same. It follows that the ESS can maintain stable performance at incidence angle $\theta \leq 40°$.

To analyze the absorption performance of this ESS visually, the absorptivity for different θ is calculated. Considering that the unit cell dimension is far less than the wavelength, grating lobes will not be presented. Therefore, the absorptivity A can be figured out from $A = 1 - |S_{11}|^2 - |S_{21}|^2$ and the results are illustrated in Fig. 8. When the low power TE wave is incident, the absorptivity is greater than 90% in the range of 5.97–13.97 GHz (except for the small flaw at 8 GHz) with a relative bandwidth about 80%. Accordingly, the relative bandwidth is close to 76% (from 5.74 to 12.82 GHz) under HPM incidence. When the TM wave is incident, a small flaw appears at 10.66 GHz and the AB is reduced by about 1.3 GHz.

In addition, the performance of ESS with respect to different polarized angles (incidence angles $\theta = 0°$) also is studied and the results are shown in Fig. 9. As shown in Fig. 9, with polarization angles φ increasing from 0° to 90°, the S-parameters of ESS basically remain the same. Therefore, the ESS for different φ has the same absorptivity as the case

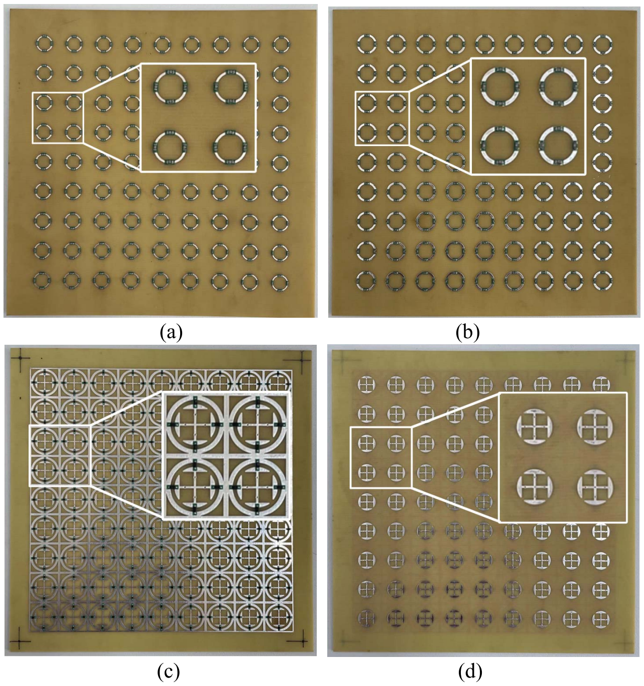

Fig. 10. Prototype of the proposed ESS. (a) Front view of absorptive layer. (b) Back view of absorptive layer. (c) Front view of switchable layer. (d) Back view of switchable layer.

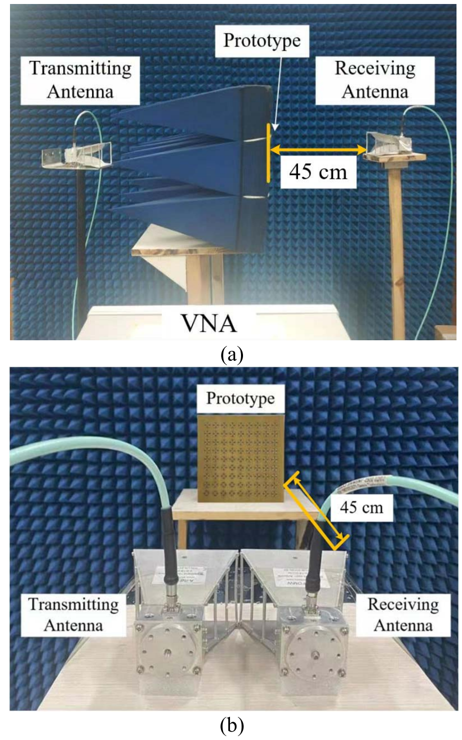

Fig. 11. Measurement setup at low power level for (a) S_{21} and (b) S_{11}.

of $\theta = 0°$ in Fig. 8. That is, the polarization insensitivity appears due to the centrosymmetric structure of the ESS unit.

III. Experimental Results

To validate the performance of ESS, a prototype with 9×9 units is fabricated and shown in Fig. 10. It has a size of 135×135 mm. Nylon screws are used to fix the absorptive layer and the switchable layer. The chip resistors and p-i-n diodes are soldered on the corresponding positions, respectively.

A. Low Power Measurement

The measurement scheme at a low power level is depicted in Fig. 11. Two horn antennas are connected to the vector network analyzer (VNA) for transmitting and receiving EM waves, respectively. The prototype is placed at the empty window of the absorbing materials for measuring S_{21}, and on the platform for measuring S_{11}. It should be noted that the two horn antennas cannot overlap in the same position in reality. So, the measured S_{11} is not completely normal incidence/reflection and measurement error will be brought. The measured and simulated S-parameters are illustrated in Fig. 12. Also, the absorptivity calculated according to Fig. 12 is presented in Fig. 13. It can be observed that the measured results match to the simulated ones. In case of $\theta = 0°$, the ESS can transmit the signal around 3.8 GHz with an IL of 0.6 dB. And its AB is 8 GHz (5.97–13.97 GHz). When the incidence angle θ increases to 40°, the passband remains stable and the absorption band shifts to 5.68–13.67 GHz. Further, the absorptivity is greater than 87% in the range of 5.97–13.97 GHz until $\theta = 40°$.

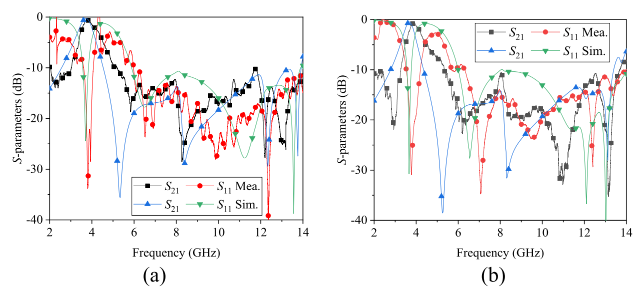

Fig. 12. Comparison of measured and simulated result at low power level. (a) $\theta = 0°$. (b) $\theta = 40°$.

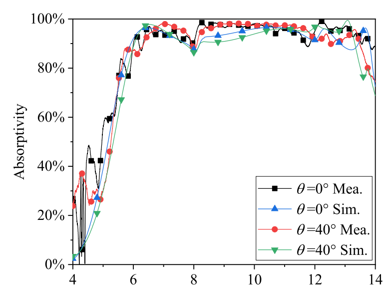

Fig. 13. Comparison of measured and simulated absorptivity at low power level.

B. High Power Measurement

To verify the shielding performance of the ESS, its S-parameters at different power level is measured. The measurement setup is depicted in Fig. 14. A 2×1 unit prototype is placed in the rectangular waveguide. An RF signal generator

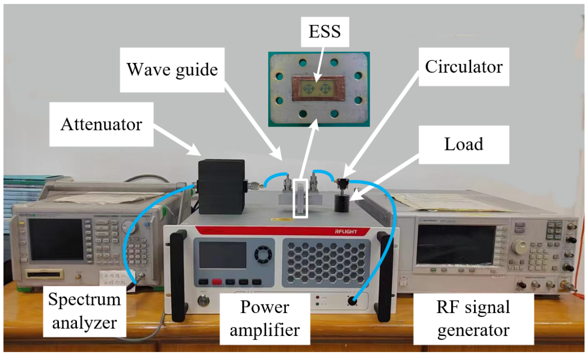

Fig. 14. Measurement setup at high power level.

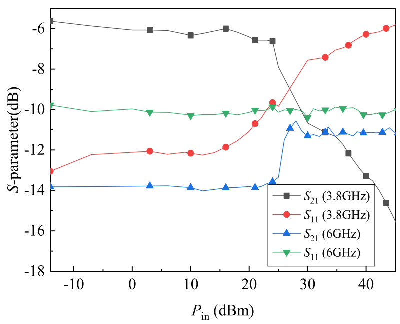

Fig. 15. Measured S-parameters of the prototype under different power levels.

and a power amplifier can produce the required HPM signals. A circulator is utilized to separate the reflection signal and a spectrum analyzer can detect the power level. As the spectrum analyzer and a matching load are connected to the output of the waveguide and circulator, respectively, the transmission signal is measured. By exchanging the spectrum analyzer and matching load, the reflection signal can be measured.

First, S-parameters are measured as input power changes and results are shown in Fig. 15. Here, two typical frequencies 3.8 GHz (central frequency of passband) and 6 GHz (in absorptivity band) are selected. At 3.8 GHz, when the input power reach to 22 dBm, S_{21} begins to decrease and S_{11} rises because some of the diodes begin to turned on. As the input power reaches to 45 dBm, the SE increases to 15 dB. At 6 GHz, S_{11} basically keeps around 11 dB. While S_{21} increases from -13.8 to -11 dB, which is match to results (after loading BC and vias) in Fig. 6. The reason for this phenomenon is that the absorptivity of ESS decreases a little under the HPM.

Then, S-parameters versus frequency are measured in case the input power is equal to 40 dBm and displayed in Fig. 16, where a reasonable agreement is found between simulated and measured results. From 3.2 to 4.5 GHz, the measured SE is basically kept around 11 dB, demonstrating the high SE to the HPM in the passband. After 5.7 GHz, S_{11} and S_{21} are less than -10 dB, demonstrating a good absorption.

It should be explained that the cross section of the waveguide becomes smaller and cannot accommodate the complete ESS unit as the frequency increases. Therefore, only

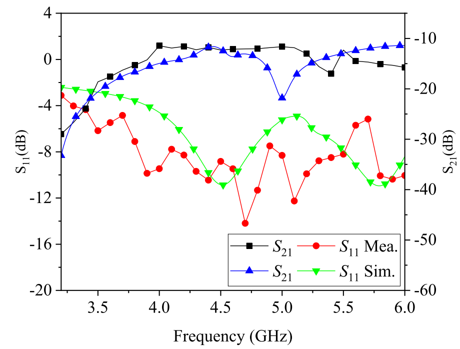

Fig. 16. Measured S-parameters versus frequency when the input power is 40 dBm.

TABLE II
COMPARISON OF PARTIAL PERFORMANCE PARAMETERS

Ref	Absorption BW		Shielding BW	Oblique incident	Profile (unit: λ_0)
	Low power	High power			
[16]	N/A	N/A	2-5 GHz, 86%	N/A	0.005
[17]	N/A	N/A	0-20 GHz, 200%	N/A	0.39
[18]	1.7-3 GHz, 55%	2.3-4.4 GHz, 63%	1.7-4.5 GHz, 90%	N/A	1.1
[19]	2.48-3.85 GHz, 43%	2.52-3.44 GHz,31%	2-4 GHz, 67%	30°	0.13
This work	5.97-13.97 GHz, 80%	5.74-12.82 GHz, 76%	0-12.8 GHz, 200%	40°	0.066

λ_0 is the free-space wavelength at the operating frequency

the S-parameters with the highest frequency up to 6 GHz are measured. Although measurements covering the whole frequency range is not carried out, the measured frequency band includes the passband and absorption band, which can also verify the design scheme to a certain extent.

Finally, the performances of the proposed ESS in this article are compared with others in references, as shown in Table II.

The proposed ESS has wider absorption and shielding bands. Besides, the lower profile and better incidence angle stability are also observed.

IV. CONCLUSION

A low-profile ESS with UWB absorption has been proposed in this article. It implements adaptive shielding utilizing p-i-n diodes and acquires absorption using resistors. Further, by introducing the BC patch and vias in the switchable layer, its shielding and AB are successfully expanded. The equivalent circuit models of switchable and absorptive layers are proposed separately to analyze the operating principle. Finally, a prototype is fabricated and measured at different power levels. The results show that the ESS can adaptively transform mode at 3.8 GHz according to the input power. Also, it can shield signal in the range of 0–12.82 GHz under HPM.

At the same time, UWB absorption is obtained in the ranges of 5.97–13.97 and 5.62–13.72 GHz in transmission/shield mode, respectively. In addition, the good angle stability and polarization insensitivity are also available.

Appendix A

A. Operating Principle of P-i-n Diode Under Microwave Signal

The response of p-i-n diode is related to the power of microwave signal. For a small microwave signal, in the positive half cycle, holes in P-region and electrons in N-region diffuse to I-region under the electric field. In I-region, some holes and electrons recombine, and a small number of them remain. When the negative half cycle of the signal comes, a small part of the remaining holes and electrons are also extracted under the electric field and return to P- and the N-region, respectively. The holes and electrons are not stored in the I-region, and its impedance will not be changed basically.

Under HPM, due to the large incident power, a large number of carriers diffused to the I-regions and the diffusion speed is fast. Although some carriers will be recombined and or extracted from I-region during the negative half cycle of the microwave signal, some carriers still cannot be extracted in a short time due to the long diffusion distance and remain in I-region. As a result, the electrical resistivity of I-region is decreased. Similarly, after the second cycle of the signal, some carriers remain in I-region. After several cycles, a large number of carriers are accumulated in I-region, and the impedance of I-region gradually decreases. Finally, the p-i-n diode is turned on.

The threshold of p-i-n diode is related to the thickness of I-region, the frequency of incident wave and the lifetime of minority carriers. The p-i-n diodes with a larger I-region thickness and shorter minority carrier life have a higher threshold. Also, the threshold will increase with frequency of incident wave.

The withstand power of p-i-n diode under HPM is not only related to its power capacity, but also to its working circuit parameters and characteristics of microwave source (continuous wave or pulse). The larger thickness of I-region and reverse breakdown voltage will result the greater withstand power.

Finally, the switching time of the p-i-n diode is related to the input power and thickness of I-region. The greater the input power is, the shorter switching time is. Under the same input power, the diode with thinner I-region has the shorter switching time.

The p-i-n diode used in this article is SMP1345-079LF, whose switching time can be controlled at about 10 ns. It has a breakdown voltage of 50 V and I-region width of 10 μm. Therefore, its breakdown electric field can be estimated as 50 V/10 μm = 5 MV/m. Through simulation we have found that the electric field generated on the 10 μm gap is about 100 kV/m when electric field of incident plane wave is 1 kV/m. Therefore, the allowed maximum electric field (incident plane wave) for the used p-i-n diode is about 50 kV/m.

Appendix B

B. Optimization Routines and Technical Details

In this article, we use CST to simulate ESS. Technical details of the simulations include the following aspects. The frequency domain solver in CST Microwave Studio is used, and Floquet boundaries are set. The EM waves propagate along the $-z$ axis. The boundaries of $X_{\max}$, $X_{\min}$, $Y_{\max}$, and $Y_{\min}$ are set to unit cell, and that of $Z_{\max}$, $Z_{\min}$ are set to open (add space). Number of Floquet modes is 2. The mesh is set to tetrahedrons.

When optimizing, every parameter of the ESS in an approximate range is swept. The following is the scanning range of several partial parameters: l_1 (2.5–4 mm), l_3 (1–3.4 mm), r_{22} (4–5.8 mm), r_{11} (3.0–4.5 mm), w_{11} (0.2–1.5 mm), r_{12} (4–7 mm), w_{12} (2.5–4 mm), and so on. The stopping criteria are that the ESS has obtained the minimum IL in the passband, the widest AB and the highest SE. In fact, it is difficult to meet all conditions and compromise is required. The priority of the three conditions is: IL $>$ SE $>$ AB.

References

[1] B. A. Munk, *Frequency Selective Surfaces: Theory and Design*. Hoboken, NJ, USA: Wiley, 2002.

[2] A. Pirhadi, H. Bahrami, and J. Nasri, "Wideband high directive aperture coupled microstrip antenna design by using a FSS superstrate layer," *IEEE Trans. Antennas Propag.*, vol. 60, no. 4, pp. 2101–2106, Apr. 2012.

[3] M. B. Yan et al., "A novel miniaturized frequency selective surface with stable resonance," *IEEE Antennas Wireless Propag. Lett.*, vol. 13, pp. 639–641, 2014.

[4] P.-S. Wei, C.-N. Chiu, C.-C. Chou, and T.-L. Wu, "Miniaturized dual-band FSS suitable for curved surface application," *IEEE Antennas Wireless Propag. Lett.*, vol. 19, no. 12, pp. 2265–2269, Dec. 2020.

[5] R. Phon, S. Ghosh, and S. Lim, "Active frequency selective surface to switch between absorption and transmission band with additional frequency tuning capability," *IEEE Trans. Antennas Propag.*, vol. 67, no. 9, pp. 6059–6067, Sep. 2019.

[6] R. Phon, S. Ghosh, and S. Lim, "Novel multifunctional reconfigurable active frequency selective surface," *IEEE Trans. Antennas Propag.*, vol. 67, no. 3, pp. 1709–1718, Mar. 2019.

[7] Q. Guo, Z. Li, J. Su, J. Song, and L. Y. Yang, "Active frequency selective surface with wide reconfigurable passband," *IEEE Access*, vol. 7, pp. 38348–38355, 2019.

[8] S. C. Bakshi, D. Mitra, and F. L. Teixeira, "Wide-angle broadband rasorber for switchable and conformal application," *IEEE Trans. Microw. Theory Techn.*, vol. 69, no. 2, pp. 1205–1216, Feb. 2021.

[9] Y. Ding et al., "Ultrawideband frequency-selective absorber designed with an adjustable and highly selective notch," *IEEE Trans. Antennas Propag.*, vol. 69, no. 3, pp. 1493–1504, Mar. 2021.

[10] J. Fang, H. Li, Q. Cao, and Y. Wang, "Study of an optically controlled active frequency selective surface," *IEEE Antennas Wireless Propag. Lett.*, vol. 17, no. 9, pp. 1707–1711, Sep. 2018.

[11] P. F. Goldsmith, "Gaussian beam propagation," in *Quasioptical Systems: Gaussian Beam Quasioptical Propogation and Applications*. Piscataway, NJ, USA: IEEE, 1998, pp. 9–38.

[12] R. Degl'Innocenti, H. Lin, and M. Navarro-Cía, "Recent progress in terahertz metamaterial modulators," *Nanophotonics*, vol. 11, no. 8, pp. 1485–1514, May 2022.

[13] C. Yang, P. Liu, and X. Huang, "A novel method of energy selective surface for adaptive HPM/EMP protection," *IEEE Antennas Wireless Propag. Lett.*, vol. 12, pp. 112–115, 2013.

[14] C. Yang et al., "Transient response of energy selective surface," *High Power Laser Part. Beams*, vol. 25, no. 4, pp. 1045–1049, 2013.

[15] Q. Zhou, P. Liu, C. Liu, N. Zhao, and R. Zheng, "A dual-band energy selective surface with hexagonal spiral structure," in *Proc. Asia–Pacific Int. Symp. Electromagn. Compat. (APEMC)*, Shenzhen, China, May 2016, pp. 8–10.

[16] N. Hu et al., “Design of ultrawideband energy-selective surface for high-power microwave protection,” *IEEE Antennas Wireless Propag. Lett.*, vol. 18, no. 4, pp. 669–673, Apr. 2019.

[17] D. Qin, R. Ma, J. Su, X. Chen, R. Yang, and W. Zhang, “Ultra-wideband strong field protection device based on metasurface,” *IEEE Trans. Electromagn. Compat.*, vol. 62, no. 6, pp. 2842–2848, Dec. 2020.

[18] J. Yuan, X. Kong, K. Chen, X. Shen, Q. Wang, and C. Wu, “Intelligent radome design with multilayer composites to realize asymmetric transmission of electromagnetic waves and energy isolation,” *IEEE Antennas Wireless Propag. Lett.*, vol. 19, no. 9, pp. 1511–1515, Sep. 2020.

[19] L. Zhou and Z. Shen, “3-D absorptive energy-selective structures,” *IEEE Trans. Antennas Propag.*, vol. 69, no. 9, pp. 5664–5672, Sep. 2021.

[20] L. M. Surhone, M. T. Tennoe, and S. F. Henssonow, *Salisbury Screen*. Beau Bassin-Rose Hill, Mauritius: Betascript Publishing, 2011.

[21] P. Rodríguez-Ulibarri, M. Navarro-Cía, R. Rodríguez-Berral, F. Mesa, F. Medina, and M. Beruete, “Annular apertures in metallic screens as extraordinary transmission and frequency selective surface structures,” *IEEE Trans. Microw. Theory Techn.*, vol. 65, no. 12, pp. 4933–4946, Dec. 2017.

[22] X. Yao, M. Bai, and J. Miao, “Equivalent circuit method for analyzing frequency selective surface with ring patch in oblique angles of incidence,” *IEEE Antennas Wireless Propag. Lett.*, vol. 10, pp. 820–823, 2011.

[23] D. Ferreira, R. Caldeirinha, I. Cuiñas, and T. Fernandes, “Square loop and slot frequency selective surfaces study for equivalent circuit model optimization,” *IEEE Trans. Antennas Propag.*, vol. 63, no. 9, pp. 3947–3955, Sep. 2015.

Wenjian Gong was born in Linfen, Shanxi, China, in 1997. He received the B.S. degree in electronic information engineering from Dalian Ocean University, Dalian, China, in 2019, and the M.S. degree in electronic and communication engineering from Shanxi University, Taiyuan, China, in 2022.

His current research interests include base station antenna, electromagnetic compatibility (EMC), and metasurface.

Wenmei Zhang (Senior Member, IEEE) was born in 1969. She received the B.S. and M.S. degrees from the Nanjing University of Science and Technology, Nanjing, China, in 1992 and 1995, respectively, and the Ph.D. degree in electronic engineering from Shanghai Jiao Tong University, Shanghai, China, in 2004.

In 2008 and 2010, she was a Senior Visiting Scholar with the Nanyang University of Technology, Singapore. She is currently a Professor with the School of Physics and Electronics, Shanxi University, Taiyuan, China. Her current research interests include microwave/millimeter wave integrated circuits, electromagnetic compatibility (EMC), and microstrip antenna. She holds 20 Chinese patents and has authored or coauthored more than 150 articles in peer-reviewed journals and over 30 papers in conference proceedings.

Prof. Zhang has served as the General Chair for “the 2019 Cross Strait Quad-Regional Radio Science and Wireless Technology Conference” and a TPC Member for multiple conferences.

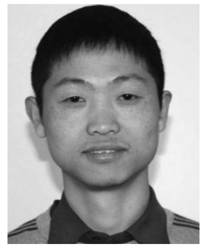

Xinwei Chen received the B.S. and Ph.D. degrees in electronic engineering from Shanxi University, Taiyuan, China, in 2002 and 2013, respectively.

He is currently an Associate Professor with the School of Physics and Electronic Engineering, Shanxi University. His current research interests include microwave and millimeter-wave passive device.

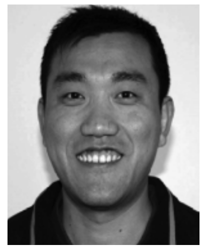

Guorui Han was born in Taiyuan, Shanxi, China, in 1977. He received the B.S. and M.S. degrees from Peking University, Beijing, China, in 2000 and 2004, respectively, and the Ph.D. degree from the College of Physics and Electronic Engineering, Shanxi University, Taiyuan, in 2013.

His current research interests include microwave-integrated circuits and multi-in multi-out (MIMO) antenna.

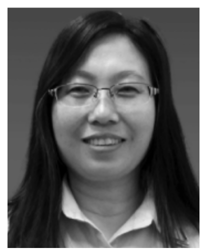

Liping Han was born in Shanxi, Shuozhou, China, in 1970. She received the B.S., M.S., and Ph.D. degrees in electronic engineering from Shanxi University, Taiyuan, China, in 1993, 2002, and 2011, respectively.

She is currently a Professor with the College of Physics and Electronics, Shanxi University. Her current research interests include microwave and millimeter-wave integrated circuits and microstrip antenna.

Jinrong Su was born in 1981. She received the B.S. and M.S. degrees in electronic engineering and the Ph.D. degree in radio physics from Shanxi University, Taiyuan, China, in 2004, 2007, and 2017, respectively.

She is currently an Associate Professor with the Department of Electronics and Information Engineering, Shanxi University. Her current research interests include through-silicon vias (TSV) modeling and the application of TSV in passive devices.

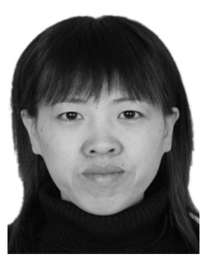

Rongcao Yang was born in Yuncheng, China, in 1970. She received the B.S. and M.S. degrees in electronics and information technology and the Ph.D. degree in optics from Shanxi University, Taiyuan, China, in 1995, 1997, and 2005, respectively.

She is currently a Professor with the College of Physics and Electronics, Shanxi University. Her current research interests include electromagnetic (EM) metamaterials, nanophotonic devices, and optical communications.